Notes on Elastic Scattering

L. Wimmer

Abstract. An overview of "Elastic Scattering of Identical Spin-Zero Nuclei" by Bromley, Kuehner and Almqvist [1].

Contents

1 Theory **2**
1.1 Classical Coulomb scattering [2] . . . 2
1.2 Coulomb scattering of 2 different particles [3] . . . 3
1.3 Mott formalism for Coulomb scattering of 2 identical particles [3] . . . 4
1.4 Blair formalism for Coulomb scattering of 2 identical particles . . . 5

2 Experimental results **6**
2.1 Figures . . . 6
2.2 Summary of the experimental results . . . 14

1 Theory

1.1 Classical Coulomb scattering [2]

Consider the scattering of two charges, Z_1e and Z_2e, with a reduced mass μ. In the lab frame, suppose the incident particle has an initial velocity of v_0, while the target particle remains stationary. Thus, the energy of the system in the CM frame can be expressed as

$$E = \frac{\mu v_0^2}{2}.$$

Let the scattering angle in the CM frame be denoted as θ, and the impact parameter as b. The motion of the system in the CM frame is described by (r, φ) and is equivalent to the reduced mass being scattered from an origin with a potential

$$V(r) = \frac{g}{r},$$

after coming with initial velocity v_0 from the infinity, where r represents the distance from the origin and

$$g = \frac{Z_1 Z_2 e^2}{4\pi\epsilon_0}$$

is a constant.

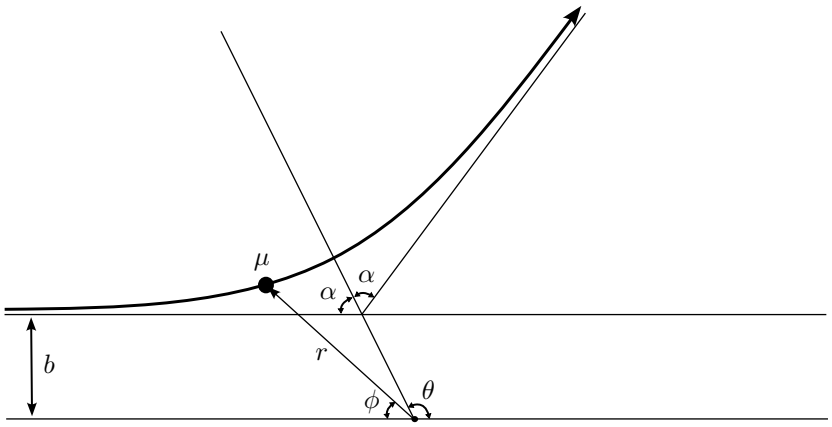

Figure 1: One-body equivalent scattering in the CM frame.

Angular momentum conservation gives

$$v_0 b = \dot{\varphi} r. \tag{1}$$

The change of the momentum before and after the scattering is

$$\Delta p = 2\mu v_0 \sin\theta/2 = \int_0^\infty \frac{g}{r^2} \sin(\theta/2 + \varphi) dt. \tag{2}$$

Plug dt from (1) into (2) and integrate from $\varphi = 0$ to $\pi - \theta$ to get

$$b = \frac{Z_1 Z_2 e^2}{8\pi\epsilon_0 E} \cot\theta/2. \tag{3}$$

The above equation relates the impact parameter and the scattering angle. Now, we will derive the classical distance of closest approach, denoted as D. At the moment of closest approach, we assume that the velocity of the reduced mass v is perpendicular to the position vector. We can use energy conservation to get

$$E = \frac{\mu v_0^2}{2} = \frac{\mu v^2}{2} + \frac{g}{D}. \tag{4}$$

Additionally, angular momentum conservation yields the equation:

$$v_0 b = vD \tag{5}$$

By combining equations (3) and (4), we can derive the expression for the distance fo closest approach:

$$\boxed{D = b\frac{\cos\left(\frac{\theta}{2}\right)}{1-\sin\left(\frac{\theta}{2}\right)} = \frac{Z_1 Z_2 e^2}{8\pi\epsilon_0 E}\left(1+\csc\frac{\theta}{2}\right)} \tag{6}$$

Now, we will derive the Rurtherford formula for the Coulomb scattering using the above results. To do so, we now assume there are two beams of particles being scattered via binary collisions. We consider the particles with impact parameter between b and $b+db$ and scattering angles between θ and $\theta+d\theta$, and we have the invertible function $b(\theta)$. We have

$$db = \left|\frac{db}{d\theta}\right| d\theta, \tag{7}$$

the range of solid angles of scattered particles

$$d\Omega(\theta) = 2\pi\sin\theta d\theta \tag{8}$$

and the cross-sectional area of the annulus of incoming particles associated to $b+db$

$$d\sigma = 2\pi b db. \tag{9}$$

Equations (3), (7), (8) and (9) together give the Rutherford formula for the Coulomb scattering:

$$\boxed{\frac{d\sigma}{d\Omega} = \left(\frac{Z_1 Z_2 e^2}{16\pi\epsilon_0 E}\right)^2 \frac{1}{\sin^4\theta/2}} \tag{10}$$

1.2 Coulomb scattering of 2 different particles [3]

In this section, we use partial wave analysis to find a solution for the Schrödinger equation

$$\left[-\frac{\hbar^2}{2\mu}\nabla^2 + \frac{Z_1 Z_2 e^2}{4\pi\epsilon_0 r}\right]\psi = E\psi \tag{11}$$

of the system of 2 different particles with reduced mass μ, charges $Z_1 e$ and $Z_2 e$, and energy E. The wave number is

$$k = \frac{\sqrt{2\mu E}}{\hbar}. \tag{12}$$

Then, we can rewrite the Schrödinger equation using parabolic coordinates (ξ, η, ϕ), assume symmetry with respect to the z-axis and use separation of variables, i.e. assume that

$$\psi(\xi,\eta) = G(\xi)H(\eta), \tag{13}$$

to get the equations

$$\frac{d}{d\xi}\xi\frac{dG(\xi)}{d\xi} + \left(\frac{k^2}{4}\xi - C\right)G(\xi) = 0 \tag{14}$$

$$\frac{d}{d\eta}\eta\frac{dH(\eta)}{d\eta} + \left(\frac{k^2}{4}\eta + C - \frac{Z_1 Z_2 e^2 m}{4\pi\epsilon_0\hbar^2}\right)H(\eta) = 0, \tag{15}$$

where C is a constant. Further analysis of boundary conditions for the incoming wave for $z \to -\infty$ gives

$$H(\eta) = e^{ik\eta/2} \tag{16}$$

and

$$G(\xi) = e^{-ik\xi/2} f(\xi) \tag{17}$$

for some function $f(\xi)$. Plug the above result into the equation for $G(\xi)$ to get

$$\xi\frac{d^2 f}{d\xi} + (1-ik\xi)\frac{df}{d\xi} - \gamma k f = 0, \tag{18}$$

where we defined

$$\gamma \equiv \frac{Z_1 Z_2 e^2 m}{4\pi\epsilon_0 \hbar^2 k}. \tag{19}$$

But it is known that the solution for the equation

$$z\frac{d^2w}{dz} + (b-z)\frac{dw}{dz} - aw = 0 \tag{20}$$

which is constant at $z = 0$ is Kummer's (confluent hypergeometric) function

$$M(a,b,z) = \sum_{s=0}^{\infty} \frac{\Gamma(a+s)\Gamma(b)z^s}{\Gamma(a)\Gamma(b+s)\Gamma(1+s)} = 1 + \frac{az}{1!b} + \frac{a(a+1)z^2}{2!b(b+1)} + \cdots, \tag{21}$$

where Γ is the gamma function. Thus, we get

$$f(\xi) \sim M(-i\gamma, 1, ik\xi). \tag{22}$$

Using some properties of the gamma function, we get the equation for $f(r)$ including terms up to $\mathrm{O}(r^{-1})$ for $z \to \infty$, which plugged back into $\psi(\xi,\eta)$ gives

$$\psi(r,\theta) \sim \left(e^{i[kz+\gamma \ln k(r-z)]} \left[1 + \frac{\gamma^2}{ik(r-z)}\right] + \frac{1}{r} f_c(\theta) e^{i[kr-\gamma \ln 2kr]} \right), \tag{23}$$

where

$$f_c(\theta) = \frac{\gamma}{2k\sin^2\theta/2} e^{-i[\gamma \ln(\sin^2\theta/2)+\pi-2\eta_0]} \tag{24}$$

is the Coulomb scattering amplitude and

$$\eta_0 = \arg\Gamma(1+i\gamma). \tag{25}$$

From the scattering amplitude, we once again get the Rutherford formula for the Coulomb scattering:

$$\boxed{\frac{d\sigma}{d\Omega} = |f_c(\theta)|^2 = \left(\frac{Z_1 Z_2 e^2}{16\pi\epsilon_0 E}\right)^2 \frac{1}{\sin^4\theta/2}} \tag{26}$$

Note that we used

$$E = \frac{\mu v_0^2}{2} = \frac{\hbar^2 k^2}{2\mu},$$

and that the result matches equation (10).

1.3 Mott formalism for Coulomb scattering of 2 identical particles [3]

Consider the scattering of two identical particles. Since they are identical, the detector cannot distinguish them and we have to consider the influence of both particles in the differential cross section. The result from the previous section clearly doesn't do that. To fix that, consider equation (23). We can rewrite it as

$$\psi(r,\theta) \sim \psi_1(r,\theta) + f_c(\theta)\psi_2(r). \tag{27}$$

If we add the wave function of the other particle, the new solution becomes

$$\psi'(r,\theta) \sim \psi_1(r,\theta) \pm \psi_1(r,\pi-\theta) + f_c(\theta)\psi_2(r) \pm f_c(\pi-\theta)\psi_2(r), \tag{28}$$

where $+$ is for bosons (symmetric wave function) and $-$ is for fermions (antisymmetric wave function). Thus, we have

$$f'(\theta) = f(\theta) \pm f(\pi-\theta) \tag{29}$$

and

$$\frac{d\sigma}{d\Omega} = |f(\theta) \pm f(\pi-\theta)|^2. \tag{30}$$

However, if the spin of a particle is denoted by s, the multiplicity of such a state is given by $2s+1$. This is because the z-component of the spin of the system can take values from $-s\hbar$ to $s\hbar$, incrementing by one unit of $\hbar$. Therefore, for the case of two identical particles with spin s, we can have $(2s+1)^2$ possible combinations for the z-component of the spins of the system with the two particles, with one singlet state (z-component of the spin of the system is zero), three triplet states (z-component of the spin of the system is $\hbar$), and so on, up to $(2s+1)$ states, where the $(4s+1)$-let has $(4s+1)$ possible states and the z-component of the spin of the system is $2s\hbar$. Note that

$$1+3+5+\cdots+(4s+1)=\sum_{t=0}^{2s}(2t+1)=(2s+1)^2. \tag{31}$$

Furthermore, if we consider the $(4t+1)$-let state whose scattering amplitude is $f_{4t+1}(\theta)$, where t takes values $0, 1/2, 1, 3/2, \ldots, s$, and note that

$$\sum_{t=0}^{2s}(2t+1)=\sum_{\substack{t=0,1,2,\ldots\\ t\leq s}}(4t+1)+\sum_{\substack{t=1/2,3/2,\ldots\\ t\leq s}}(4t+1), \tag{32}$$

we find that the singlet state is associated to a pair of bosons ($t=0$), a triplet is associated to a pair of fermions ($t=1/2$), and so on. Therefore, using the result from our previous analysis of the wave function, we know that, for fermions ($t=1/2, 3/2, \ldots$),

$$\frac{d\sigma}{d\Omega}\Big|_{4t+1}=|f_{4t+1}(\theta)-f_{4t+1}(\pi-\theta)|^2. \tag{33}$$

On the other hand, for bosons ($t=0, 1, 2, \ldots$),

$$\frac{d\sigma}{d\Omega}\Big|_{4t+1}=|f_{4t+1}(\theta)+f_{4t+1}(\pi-\theta)|^2. \tag{34}$$

Since

$$f_{4t+1}(\theta)=f_c(\theta)$$

for all values of t, the weighted differential cross section becomes

$$\frac{d\sigma}{d\Omega}=\frac{1}{(2s+1)^2}\left(\Big|f_c(\theta)+f_c(\pi-\theta)\Big|^2+3\Big|f_c(\theta)-f_c(\pi-\theta)\Big|^2+\cdots+(4s+1)\Big|f_c(\theta)+(-1)^{2s}f_c(\pi+\theta)\Big|^2\right),$$

where $f_c(\theta)$ is the Coulomb scattering amplitude as in (24). After some simplifications, we get

$$\frac{d\sigma}{d\Omega}=|f_c(\theta)|^2+|f_c(\pi-\theta)|^2+(-1)^{2s}\frac{2}{2s+1}\left[f_c(\theta)f_c^*(\pi-\theta)+f_c^*(\theta)f_c(\pi-\theta)\right]. \tag{35}$$

Plugging (24) into the above equation, we get the Mott differential cross section:

$$\boxed{\left.\frac{d\sigma}{d\Omega}\right|_{\text{Mott}}=\left(\frac{Z_1Z_2e^2}{16\pi\epsilon_0E}\right)^2\left|\csc^4\frac{\theta}{2}+\sec^4\frac{\theta}{2}+(-1)^{2s}\frac{2}{2s+1}\cos\left[\frac{(Ze)^2}{\hbar v_0}\ln\left(\tan^2\frac{\theta}{2}\right)\right]\csc^2\frac{\theta}{2}\sec^2\frac{\theta}{2}\right|} \tag{36}$$

1.4 Blair formalism for Coulomb scattering of 2 identical particles

The Blair is a modification of the Mott formalism to consider the nuclear potential between particles, which becomes relevant at high energies and is not accounted for in the Mott formalism. It introduces the concept that all partial waves in the incident beam, with an impact parameter corresponding to a classical distance of closest approach smaller than the nuclear interaction radius, are completely absorbed. In contrast, partial waves with larger impact parameters undergo pure Coulomb scattering.

By incorporating these considerations, the Blair formalism provides a more comprehensive description of scattering phenomena at high energies. Blair model's differential cross section can be expressed as:

$$\left.\frac{d\sigma}{d\Omega}\right|_{\text{Blair}} = \left(\frac{(Ze)^2}{16\pi\epsilon_0 E}\right)^2 \Bigg| \exp(2i\delta_0)\csc^2\frac{\theta}{2}\exp\left(-i\eta\ln\sin^2\frac{\theta}{2}\right) \pm \exp(2i\delta_0)\sec^2\frac{\theta}{2}\exp\left(-i\eta\ln\cos^2\frac{\theta}{2}\right) - \frac{i}{\eta}\sum_{l=0}^{l_{max}}(2l+1)\exp(2i\delta_l)P_l(\cos\theta) \mp \frac{i}{\eta}\sum_{l=0}^{l_{max}}(2l+1)\exp(2i\delta_l)P_l(-\cos\theta)\Bigg|^2 \tag{37}$$

Here, θ represents the center-of-mass scattering angle, δ_l denotes the Coulomb phase of order l, P_l corresponds to the Legendre polynomials, and η is the Sommerfeld number given by:

$$\eta = \frac{(Ze)^2}{\hbar v_0}.$$

2 Experimental results

2.1 Figures

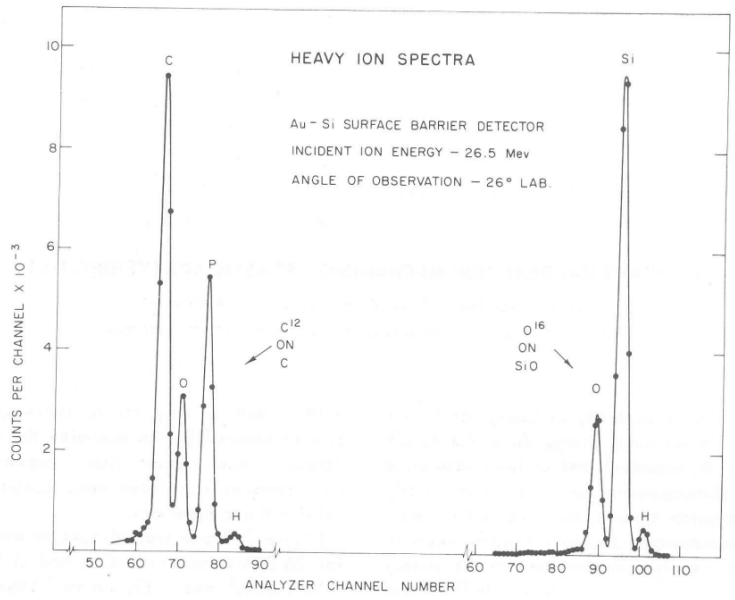

Figure 2: Energy spectra measured at 26° for 26.5 MeV beams of C^{12} and O^{16} incident on ~ 50 $\mu g/cm^2$ and ~ 100 $\mu g/cm^2$ targets of carbon and silicon monoxide, respectively. Horizontal axis is associated to energy and vertical axis associated to the number of particles detected.

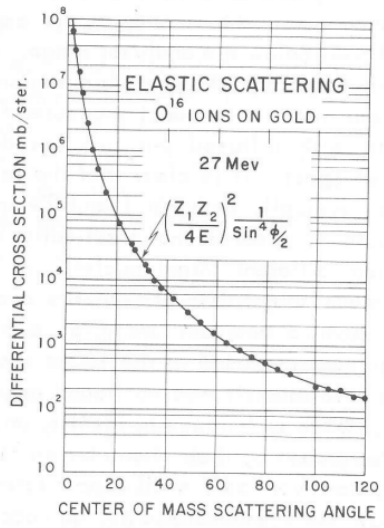

Figure 3: Rutherford formula for the relation between differential cross section and scattering angle agrees with experimental data for elastic scattering of O^{16} ions on gold.

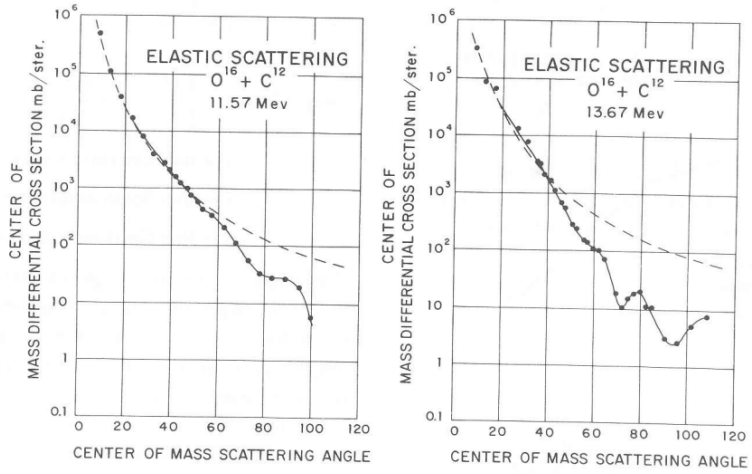

Figure 4: Relation between differential cross section and scattering angle for the elastic scattering of O^{16} $+C^{12}$ with 11.57 MeV and 13.67 MeV. In the forwards angles, the experimental data does not align with the Rutherford formula. However, the oscillatory structure after the decrease and the small exceeding of the Rutherford formula before the decrease are characteristics predicted by the Blair model.

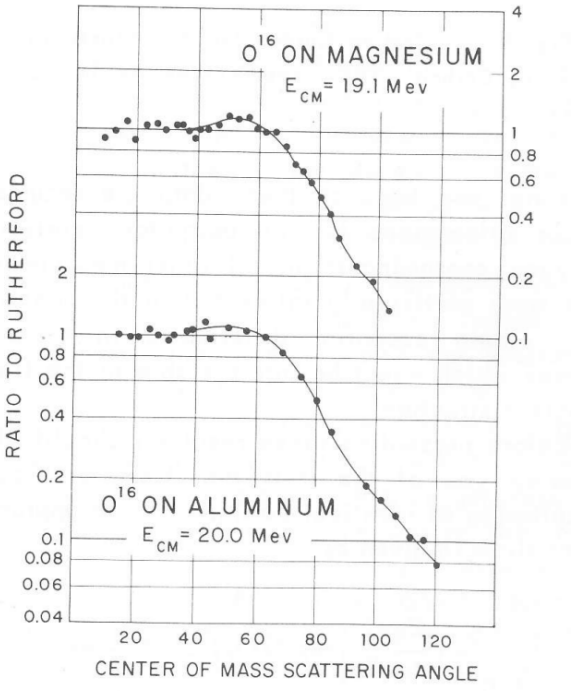

Figure 5: Angular distributions of O^{16} ions on magnesium and aluminum, demonstrating agreement with the Rutherford formula even at forward angles.

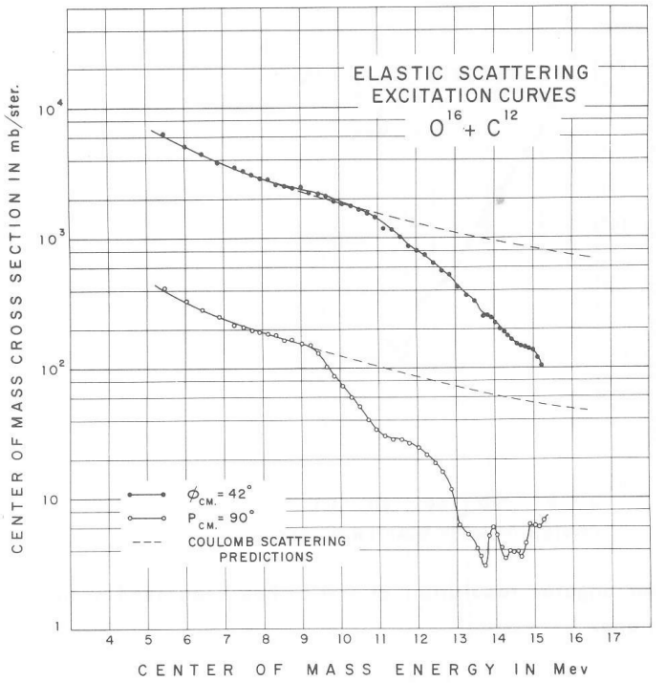

Figure 6: Relation between differential cross section and the CM energy for the elastic scattering of O^{16}+C^{12} for ϕ_{CM} =42 and 90°. Dashes lines are the E^{-2} predictions from Rutherford formula. The experimental data deviates from the Rutherford formula at higher energies due to the Coulomb barrier. As the incident particle's energy increases, it can overcome the Coulomb repulsion and approach the target nucleus more closely, where the nuclear potential is effective. This leads to a deviation from the predictions of the Rutherford formula for higher energies. The 42°data shows less oscillatory structure because it has larger classical distance of closest approach (equation (6)) and thus is less affected by some nuclear potential.

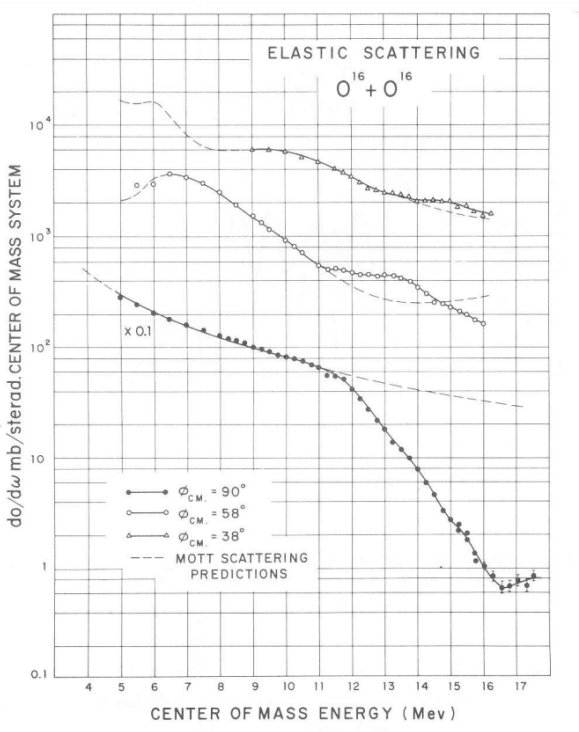

Figure 7: Relation between differential cross section and energy for O^{16}+O^{16} elastic scattering for different angles. We can use Mott formalism to check the experimental data since it is an elastic scattering of 2 identical particles. For $\phi = 90°$, the energy modulation (energy dependence of the third term of the Mott differential cross section) disappears and data aligns considerably well with the Mott formalism, except for extreme energies. The data for all three angles conforms to the Mott formalism for energies below 10.5 MeV. However, beyond this energy threshold, the graph exhibits a rapid decline, primarily attributed to nuclear interactions.

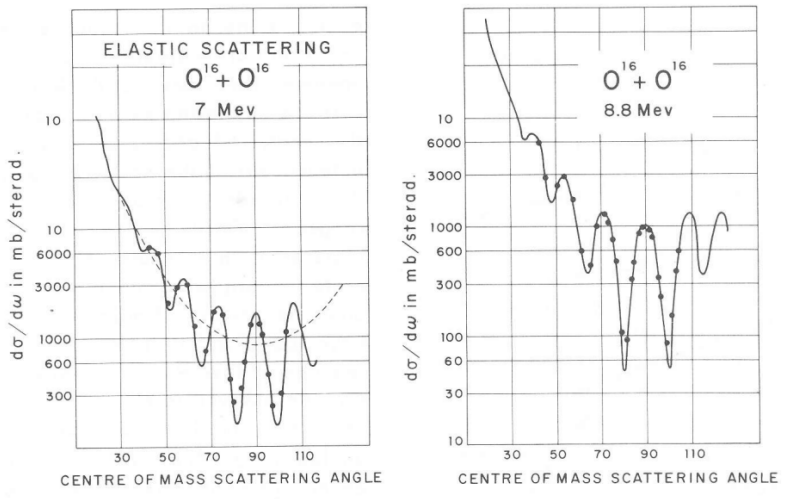

Figure 8: Relation between differential cross section and scattering angle for O^{16}+O^{16} elastic scattering at 7 MeV and 8.8 MeV. The solid curve represents a sketch of the data curve, while the dashed curve represents the Rutherford prediction. The experimental data oscillates around the Rutherford prediction, but it does not match Mott or Blair predictions.

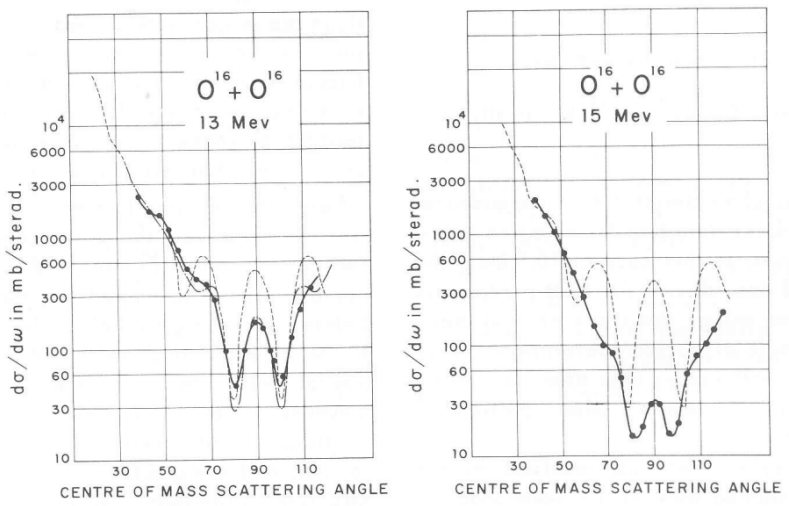

Figure 9: Relation between differential cross section and scattering angle for O^{16}+O^{16} elastic scattering at 13 MeV and 15 MeV.The solid curve represents a sketch of the data curve, while the dashed and dot-dashed curves represent the Mott prediction and the Blair prediction for $l_{max} = 6$, respectively. At 13 MeV, Blair aligns better with data than Mott, notably at around 60° and 110°. At 15 MeV, data is below Mott for most angles and doesn't match either prediction.

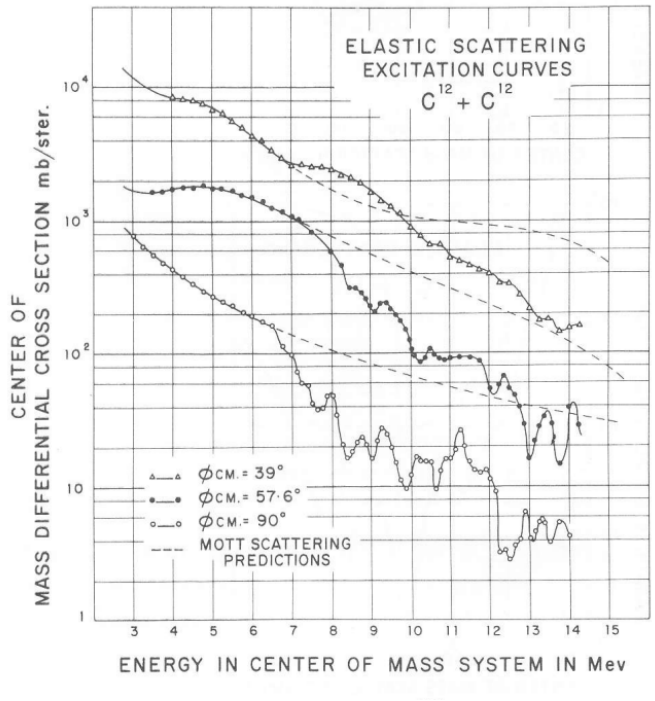

Figure 10: Relation between differential cross section and energy for the elastic scattering of C^{12}+C^{12} for different angles. As before, the Mott predictions are in accord with the experimental data before the Coulomb barrier. However, in contrast to the oxygen results, for energies above the barrier, the cross sections do not decrease in roughly exponential fashion and unexpectedly show marked resonance structure.

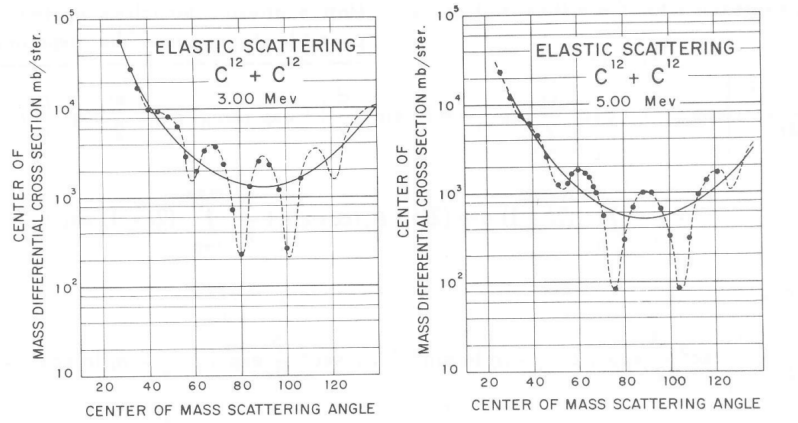

Figure 11: Angular distributions for C^{12}+C^{12}. The solid and dashed curves are the Rutherford and Mott predictions, respectively. The data aligns perfectly with the Mott prediction.

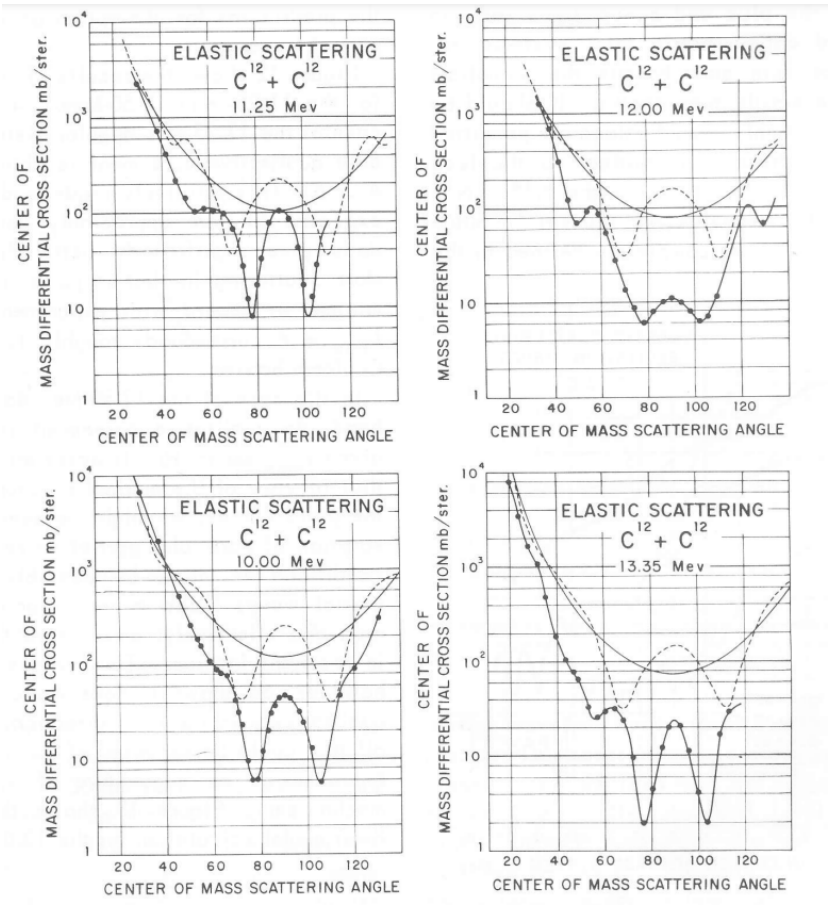

Figure 12: Angular distributions for C^{12}+C^{12}. Data curve (dark solid) is predominantly shifted below the Mott prediction (dashed), while the Rutherford prediction (light solid) is also depicted.

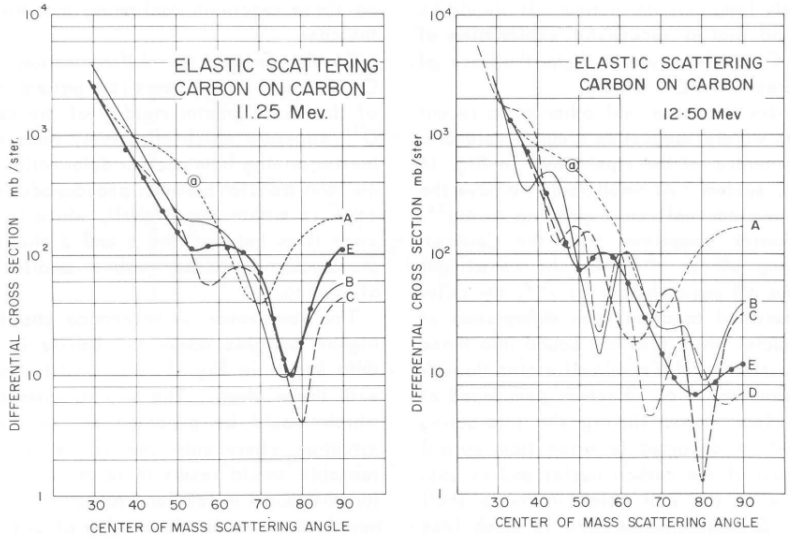

Figure 13: Blair model predictions for C^{12}+C^{12}. A and E are the Mott and experimental curves, respectively. In the left figure, B and C correspond to Blair's model for $l_{max} = 4$ and 6, respectively. In the right figure, C corresponds to $l_{max} = 8$, B corresponds to $l_{max} = 6 + l = 10$, and D corresponds to $l_{max} = 4 + l = 8$. In the case of 11.25 MeV, reasonable qualitative agreement is obtained for $l_{max} = 4$ or 6, better than the Mott model. As for the 12.50 MeV data, no qualitative agreement is found for any given l_{max} up to 16.

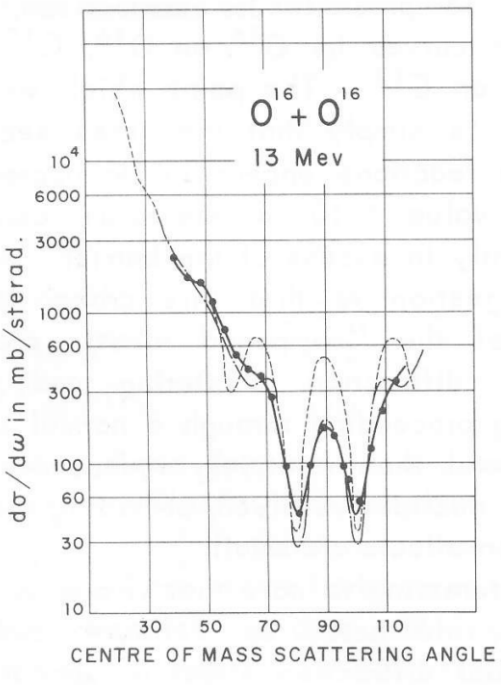

Figure 14: Blair model predictions for the 13.0 MeV O^{16}+O^{16} angular distribution. The dashed, broken, and full curves are the Mott and Blair predictions and the experimental data, respectively. The data aligns with the Blair model for $l_{max} = 6$.

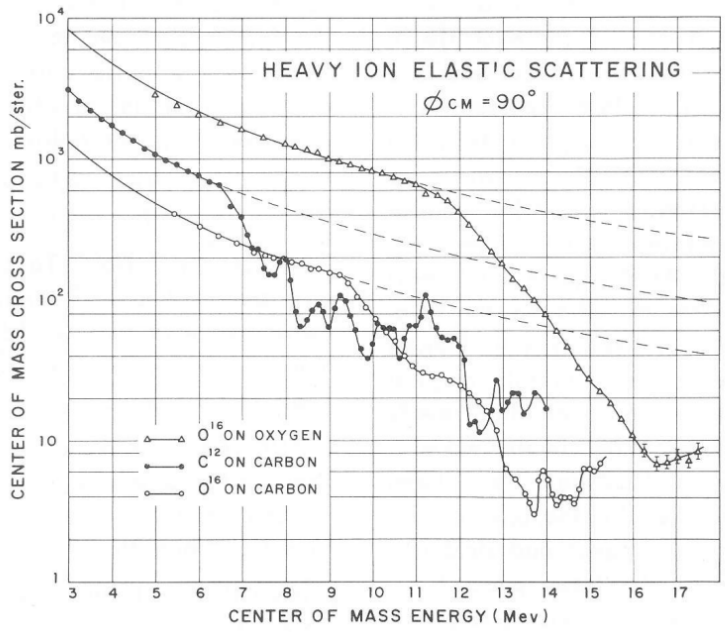

Figure 15: Comparison of the O+O, O+C, and C+C 90°excitation curves. The cross sections for all three reactions appear to be approaching a common value of $\sim$ 10 mb/steradian at energies significantly in excess of the barrier. This suggests that this cross section is typical of the "compound elastic processes" including diffraction scattering and potential scattering proceeding through a normal compound system, and thus relatively independent of the particular nuclides involved (providing that barrier penetration effects are small).

2.2 Summary of the experimental results

Experimental data for the elastic scattering of C+C and O+O at different energies was analysed. At energies below the Coulomb barrier, the measurements of both angle and energy exhibit excellent agreement with the Mott scattering predictions. However, above the Coulomb barrier, the excitation curve for O+O drops exponentially below the Mott predictions, reaching a value of 10 mb/sr at 16.5 MeV, and remains relatively constant thereafter. In contrast, the excitation curve for C+C displays marked resonant interference structures. The Blair model provides improved predictions for the angular distributions of C+C scattering at 11.25 MeV and O+O scattering at 13 MeV compared to the Mott model.

References

[1] DA Bromley, JA Kuehner, and E Almqvist. Elastic scattering of identical spin-zero nuclei. *Physical Review*, 123(3):878, 1961.

[2] T Watkins. The derivation of the rutherford scattering formula and its generalization. https://www.sjsu.edu/faculty/watkins/scattering.htm. Accessed: 2023-06-15.

[3] 石飛由介、岡田健、桑野将大、杉本太郎、吉田登志輝. ラザフォード散乱. http://ppwww.phys.sci.kobe-u.ac.jp/seminar/pdf/Rutherford2016.pdf. Accessed: 2023-06-15.